Combining Ligand-Based Pharmacophore Modeling, Quantitative Structure−Activity Relationship Analysis and in Silico Screening for the Discovery of New Potent Hormone Sensitive Lipase Inhibitors

Mutasem O. Taha,*[,†] Lina A. Dahabiyeh,[†] Yasser Bustanji,[‡] Hiba Zalloum,[†] and Suhair Saleh[§]

Department of Pharmaceutical Sciences, Faculty of Pharmacy, University of Jordan, Amman, Jordan, Department of Biopharmaceutics and Clinical Pharmacy, Faculty of Pharmacy, University of Jordan, Amman, Jordan, Department of Pharmaceutical Sciences and Pharmaceutics, Applied Science University, Amman, Jordan

Received June 14, 2008

Hormone sensitive lipase (HSL) has been recently implicated in diabetes and obesity, prompting attempts to discover new HSL inhibitors. Toward this end, we explored the pharmacophoric space of HSL inhibitors using four diverse sets of compounds. Subsequently, genetic algorithm and multiple linear regression analysis were employed to select optimal combination of pharmacophoric models and 2D physicochemical descriptors capable of yielding a self-consistent and predictive quantitative structure−activity relationship (QSAR) ($r = 0.822$, $n = 99$, $F = 11.1$, $r^2_{LOO} = 0.521$, r^2_{PRESS} against 23 external test inhibitors = 0.522). Interestingly, two pharmacophoric models emerged in the QSAR equation suggesting at least two binding modes. These pharmacophores were employed to screen the National Cancer Institute (NCI) list of compounds and our *in-house* built database of established drugs and agrochemicals. Active hits included the safe herbicidal agent bifenox ($IC_{50} = 0.43$ μM) and the nonsteroidal anti-inflammatory naproxen ($IC_{50} = 1.20$ μM). Our active hits undermined the traditional believe that HSL inhibitors should possess covalent bond-forming groups.

1. Introduction

1.1. Hormone Sensitive Lipase. Recent years have witnessed a flurry of new oral drugs for the treatment of type 2 diabetes and obesity. The impetus for developing new antidiabetic drugs comes from the unmet need for pharmacological tools that allow diabetic patients to achieve recommended glucose control targets more effectively and safely.[1]

Elevated free fatty acids plasma levels (FFAs) are thought to play a major role in the pathogenesis of insulin resistance and type 2 diabetes by inhibiting glucose uptake and utilization by muscles.[2−4] Furthermore, chronic hyperglycemia is usually accompanied by abnormalities in lipid metabolism. Both factors prompted continued interest in the role played by FFA in the pathogenesis of diabetes.[3,5]

HSL[a] is a neutral lipase that has broad substrate specificity; it catalyzes the hydrolysis of triacylglycerol, diacylglycerol, monoacylglycerol, and cholesteryl esters as well as retinyl esters. For that reason, HSL is not only present in adipose tissues but is also found in tissues in which cholesterol esters are stored, e.g., adrenal cortex, ovaries, testis, and heart.[6]

HSL is a component of the metabolic switch between glucose and FFAs as energy sources. Adipose HSL activity is normally inhibited by insulin. However, HSL remains active in type 2 diabetes, despite elevated insulin levels, presumably through loss of insulin's inhibitory effect. The resulting fatty acid flux stimulates inappropriate hepatic gluconeogenesis.[6,7] Furthermore, high FFA levels are suspected to play a role in the mechanisms of insulin resistance itself.[8]

Adipocyte HSL is composed of two major structural domains, an *N*-terminal domain, which is variable between isoforms, and a *C*-terminal catalytic domain, which is identical in all known HSL isoforms. The function of the *N*-terminal domain is poorly understood, still, it has been implicated in protein−protein and protein−lipid interactions. The catalytic domain harbors the active site, including the residues of the catalytic triad Asp703 His733, and Ser423, as well as a regulatory module including the phosphorylation sites of HSL.[9]

The central role of HSL in regulating fatty acid metabolism makes it an interesting pharmacological target for the treatment of insulin resistance and dyslipidemic disorders where a decrease in delivery of fatty acids to the circulation and thereby reducing insulin resistance is desirable.[6−8,10−12] During the last couple of years, a range of different classes of HSL inhibitors have been described by different companies. Bayer has published work on 2*H*-isoxazol-5-ones.[7] Aventis has published work on oxadiazolones.[13,14] Ontogene has published work on pyrrolopyrazinediones,[12] and Novo Nordisk has published work on carbazates,[15] carbamoyltriazoles,[10] and aryl boronic acids.[16]

The continued interest in the development of new HSL inhibitors combined with the lack of available HSL crystallographic structures and adequate computer-aided drug discovery efforts in this area[44] prompted us to explore the possibility of developing ligand-based three-dimensional (3D) pharmacophore(s) integrated within self-consistent QSAR model for HSL inhibitors. The pharmacophore model(s) can be used as 3D search query(ies) to mine 3D libraries for new HSL inhibitors, while the QSAR model helps to predict the biological activities of the captured compounds and therefore prioritize them for in vitro evaluation.

* To whom correspondence should be addressed. Phone: 00962 6 5355000, ext. 23305. Fax: 00962 6 5339649. E-mail: mutasem@ju.edu.jo.

† Department of Pharmaceutical Sciences, Faculty of Pharmacy, University of Jordan.

‡ Department of Biopharmaceutics and Clinical Pharmacy, Faculty of Pharmacy, University of Jordan.

§ Department of Pharmaceutical Sciences and Pharmaceutics, Applied Science University.

[a] Abbreviations: HSL: hormone sensitive lipase; QSAR: quantitative structure−activity relationship; MLR: multiple linear regression; GA: genetic algorithm; HBA: hydrogen bond acceptor; HBD: hydrogen bond donor.

10.1021/jm800718k CCC: $40.75
Published on Web 09/20/2008

We employed the HYPOGEN module from the CATALYST software package[17] to construct plausible binding hypotheses for HSL inhibitors. Subsequently, genetic function algorithm (GFA) and multiple linear regression (MLR) analyses were employed to search for an optimal QSAR that combine high-quality binding pharmacophores with other molecular descriptors and capable of explaining bioactivity variation across a collection of diverse HSL inhibitors. The optimal pharmacophores were subsequently used as 3D search queries to screen NCI list of compounds and our *in-house* built structural database of established drugs and agrochemicals for new HSL inhibitors.

CATALYST models drug−receptor interaction using information derived only from the drug structure.[17−25] HYPOGEN identifies a 3D array of a maximum of five chemical features common to active training molecules, which provides a relative alignment for each input molecule consistent with their binding to a proposed common receptor site. The chemical features considered can be hydrogen bond donors and acceptors (HBDs and HBAs), aliphatic and aromatic hydrophobes, positive and negative charges, positive and negative ionizable groups, and aromatic planes. The conformational flexibility of training ligands is modeled by creating multiple conformers, judiciously prepared to emphasize representative coverage over a specified energy range. CATALYST pharmacophores have been used as 3D queries for database searching and in 3D-QSAR studies.[26−31]

2. Results and Discussion

CATALYST enables automatic pharmacophore construction by using a collection of molecules with activities ranging over a number of orders of magnitude. CATALYST pharmacophores (hypotheses) explain the variability of bioactivity with respect to the geometric localization of the chemical features present in the molecules used to build it. The pharmacophore model consists of a collection of features necessary for the biological activity of the ligands arranged in 3D space.

Different hypotheses were generated for a series of HSL inhibitors. A total of 122 compounds were used in this study (Figure 1 and Table 1). Four training subsets were selected from the collection (Table 2). Each subset consisted of inhibitors of wide structural diversity. The biological activity in the training subsets spanned from 3.5 to 4.0 orders of magnitude. Genetic algorithm and multiple linear regression statistical analysis were subsequently employed to select an optimal combination of complementary pharmacophores capable of explaining bioactivity variations among all collected inhibitors.

2.1. Data Mining and Conformational Coverage. The literature was surveyed to collect many structurally diverse reported HSL inhibitors (**1**−**122**, see Table 1 and Figure 1).[7,10] The 2D structures of the inhibitors were imported into CATALYST and converted automatically into plausible 3D single conformer representations. The resulting single conformer 3D structures were used as a starting point for conformational analysis and in the determination of various molecular descriptors for QSAR modeling.

The conformational space of each inhibitor was extensively sampled utilizing the poling algorithm employed within the CONFIRM module of CATALYST.[22] Conformational coverage was performed employing the "Best" module to ensure extensive sampling of conformational space. Efficient conformational coverage guarantees minimum conformation-related noise during pharmacophore generation and validation stages. Pharmacophore generation and pharmacophore-based search procedures are known for their sensitivity to inadequate conformational sampling within training compounds.[32]

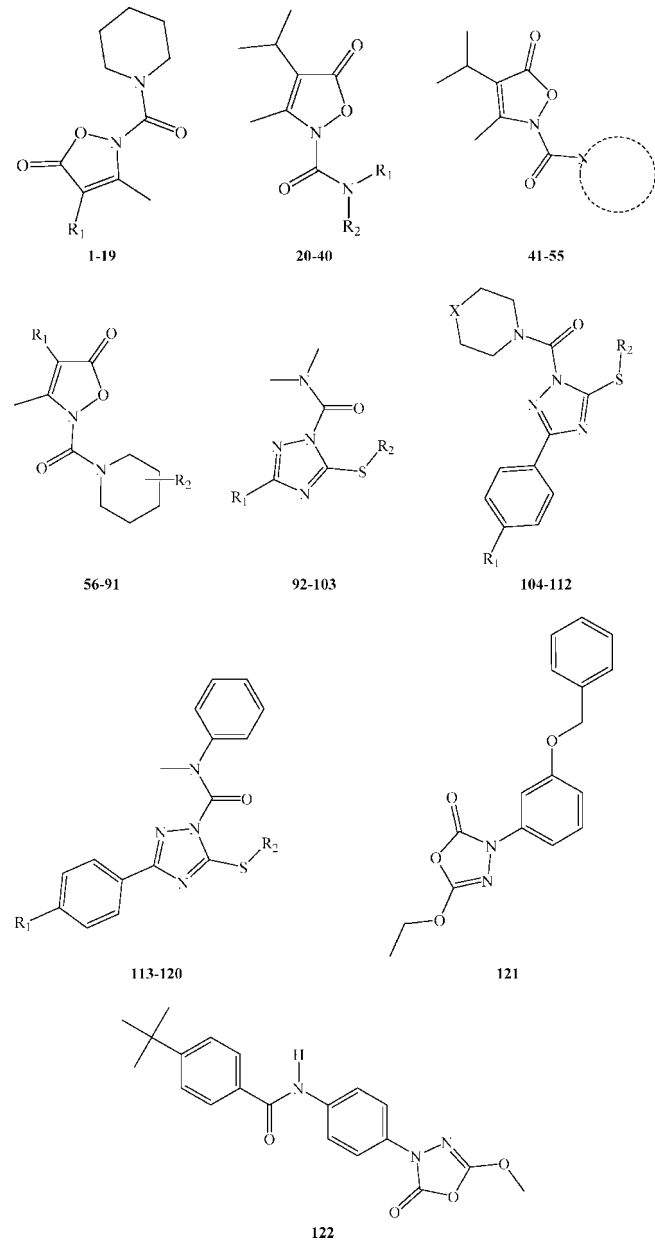

Figure 1. The chemical scaffolds of training compounds; the detailed structures are as in Table 1.

2.2. Exploration of HSL Pharmacophoric Space. CATALYST-HYPOGEN enables automatic pharmacophore construction by using a collection of at least 16 molecules with bioactivities spanning over 3.5 orders of magnitude.[17,21−25] Accordingly, as we have an informative list of 122 HSL inhibitors of evenly spread bioactivities over more than 3.5 orders of magnitude, this prompted us to employ CATALYST-HYPOGEN to identify possible pharmacophoric binding modes assumed by different HSL inhibitors.

HYPOGEN implements an optimization algorithm that evaluates large number of potential binding models for a particular target through fine perturbations to hypotheses that survived the constructive and subtractive phases of the modeling algorithm (see Section 4.1.4, Pharmacophoric Hypotheses Generation in the Experimental Section).[21] The extent of the evaluated pharmacophoric space is reflected by the configuration (config) cost calculated for each modeling run. It is generally recommended that the config cost of any HYPOGEN run not exceed

Table 1. Structures of HSL Inhibitors Utilized in Modeling; the Corresponding Scaffolds are in Figure *1*

no.	R1	R2	cyclic amine	X	IC_{50}(nM)
1	*S*-4-chlorophenyl				6
2	SO_2(4-chloro)phenyl				35
3[a]	*S*-phenyl				6
4[a]	benzyl				5
5	CH_3				13
6	ethyl				18
7	*n*-butyl				7
8	isopropyl				2
9	isobutyl				5
10	*tert*-butyl				14
11	cyclopentyl				6
12[a]	cyclohexyl				11
13	4-tetrahydropyranyl				71
14	4-tetrahydrothiopyrany				11
15	4-tetrahydrothiopyranyl dioxide				55
16	$CH_2CH_2OCH_3$				10
17	CH_2CH_2OPh				4
18	CH_2(*N*-CH_3)-2-indolyl				17
19	phenyl				14
20[a]	H	*tert*-butyl			>1000
21	H	phenyl			>1000
22	H	8-quinolinyl			N/A[b]
23[a]	H	CH_2cyclohexyl			72
24	CH_3	cyclohexyl			9
25	CH_3	benzyl			5
26	CH_3	(2-fluoro)benzyl			4
27	CH_3	(3-fluoro)benzyl			5
28	CH_3	(4-fluoro)benzyl			111
29	CH_3	(4-methyl)benzyl			408
30[a]	CH_3	CH_2(2-furanyl)			4
31	CH_3	CH_2(2-thienyl)			2
32	CH_3	CH_2CH_2CN			>1000
33	CH_3	CH_2CH_2Ph			180
34	CH_3	CH_2CH_2 (2-indolyl)			N/A[b]
35	CH_3	CH_2CONH_2			>1000
36[a]	CH_3	phenyl			7
37	CH_3	4-chlorophenyl			17
38	CH_3	2-pyridyl			240
39[a]	ethyl	ethyl			1400
40	isopropyl	isopropyl			N/A[b]
41			pyrrolidine		15
42			2,5-dimethylpyrrolidine		N/A[b]
43			3-pyrroline		72
44			indoline		>1000
45			tetrahydroquinoline		60
46			piperazine		>1000
47			*N*-methylpiperazine		314
48			*N*-benzylpiperazine		65
49			*N*-phenylpiperazine		6
50			*N*-(2-chlorophenyl)piperazine		30
51			*N*-(2-pyrimidinyl) piperazine		67
52			morpholine		52
53[a]			thiomorpholine		8
54[a]			homopiperidine		62
55			azacyclooctane		900
56	isopropyl	2-methyl			93
57[a]	isopropyl	3-(*R*)-methyl			20
58	isopropyl	3-(*S*)-methyl			3
59[a]	isopropyl	3-hydroxymethyl			180
60[a]	isopropyl	3-$CON(Et)_2$			>1000
61[a]	isopropyl	3-CO2Et			28
62	isopropyl	4-methyl			6
63	*n*-butyl	4-methyl			1
64	isobutyl	4-methyl			3
65	cyclohexyl	4-methyl			4
66	CH_2CH_2OEt	4-methyl			3
67	4-tetrahydrothiopyranyl	4-methyl			6
68	isopropyl	4-benzyl			102
69	isopropyl	4-phenyl			12
70	isobutyl	4-phenyl			10
71	cyclopentyl	4-phenyl			24
72	$CH_2CH_2OCH_3$	4-phenyl			11
73	isopropyl	4-(3-fluorophenyl)			12
74	$CH_2CH_2OCH_3$	4-(3-fluorophenyl)			20
75	$CH_2CH_2OCH_3$	4-(3-methylphenyl)			23

Table 1. Countinued

no.	R1	R2	cyclic amine	X	IC_{50}(nM)
76	isopropyl	4-(4-methylphenyl)			37
77	isopropyl	4-(4-CF_3-phenyl)			160
78	isopropyl	4-(4-*tert*-bu-phenyl)			480
79	isopropyl	4-COphenyl			250
80	isopropyl	4-CO_2Et			6
81	isopropyl	4-hydroxy			166
82	isopropyl	4-keto			200
83	isopropyl	4-CON(CH_3)2			>1000
84	isopropyl	4-(4-CH_3-2-isoxazoyl)			28
85	isopropyl	4-(5-CH_3-2-oxadiazolyl)			>1000
86[a]	isopropyl	4-*N*-piperidinyl			N/A[b]
87	isopropyl	2,5-dimethyl			460
88	isopropyl	3,3-dimethyl			7
89[a]	isopropyl	3,5-dimethyl			326
90	isopropyl	4-CN-4-phenyl			>1000
91	isopropyl	4-OH-4-phenyl			>1000
92	4-chlorophenyl	methyl			0.353
93	4-chlorophenyl	ethyl			3.71
94	4-chlorophenyl	propyl			1.06
95	4-methylphenyl	methyl			0.53
96	4-methylphenyl	1,1,1-trifluoro-ethyl			10.59
97	4-methylphenyl	hexane			882.35
98[a]	4-trifluoromethoxyphenyl	methyl			1.76
99[a]	4-methoxyphenyl	methyl			15.88
100	4-trifluoromethylphenyl	methyl			1.76
101	biphenyl	methyl			26.47
102	naphthalene	methyl			35.29
103	vinyl-benzene	methyl			882.35
104[a]	Cl	methyl		O	35.29
105[a]	Cl	1,1,1-triflouro-ethyl		O	158.82
106[a]	Cl	hexane		O	882.35
107	methyl	methyl		O	70.59
108	methoxy	ethyl		O	158.82
109	Cl	methyl		CH_2	1.76
110	Cl	1,1,1-triflouro-ethyl		CH_2	7.06
111	Cl	methylcyclopropyl		CH_2	3.53
112	Cl	hexane		CH_2	882.35
113[a]	Cl	methyl			2.82
114	Cl	1,1,1-triflouroethyl			3
115	Cl	methylcyclopropyl			1.09
116	Cl	hexane			7.06
117	methyl	methyl			1.76
118[a]	methyl	hexane			12.35
119	trifluoromethoxy	methyl			4.41
120	methoxy	ethyl			5.29
121					19.41
122					0.41

[a] These compounds were employed as the external testing subset in QSAR modeling. [b] N/A = not active.

Table 2. Training Subsets Employed in Exploring the Pharmacophoric Space of HSL Inhibitors; Numbers Correspond to Compounds in Table *1* and Figure *1*

training subsets	most active[a]	moderately active	least active[b]
A	109, 114, 122	3, 17, 19, 23, 24, 26, 30, 36, 37, 38, 45, 51, 52, 68, 80, 83, 99, 102, 103, 118, 119, 121	39, 40
B	8, 31, 92, 109, 113	1, 6, 17, 20, 33, 36, 49, 70, 80, 103, 104, 111	39, 40
C	66, 92, 98, 115	2, 13, 19, 21, 23, 24, 30, 32, 47, 48, 49, 61, 81, 83, 87, 90, 101, 103, 104, 120, 121	39, 40
D	31, 66, 122	1, 13, 16, 18, 19, 21, 28, 33, 43, 51, 61, 69, 84, 121	39, 40

[a] Potency categories as defined by eqs 2 and 3 in Section 4.1.4, Pharmacophoric Hypotheses Generation under the Experimental Section. [b] Potency categories as defined by equations 2 and 3 in Section 4.1.4, Pharmacophoric Hypotheses Generation under the Experimental Section.

17 (corresponding to two[17] hypotheses to be assessed by CATALYST) to guarantee thorough analysis of all models.[22]

The size of the investigated pharmacophoric space is a function of training compounds, selected input chemical features, and other CATALYST control parameters.[22] Restricting the extent of explored pharmacophoric space should improve the efficiency of optimization via allowing effective evaluation of limited number of pharmacophoric models. On the other hand, extensive restrictions imposed on the pharmacophoric space might reduce the possibility of discovering optimal pharmacophoric hypotheses, as they might occur outside the "boundaries" of the pharmacophoric space.

Therefore, we decided to explore the pharmacophoric space of HSL inhibitors under reasonably imposed "boundaries" through 16 HYPOGEN automatic runs conduct by employing four carefully selected training subsets (i.e., from the collected compounds): subsets A, B, C, and D in Table 2. The training compounds in these subsets were selected in such away to guarantee maximal 3D diversity and continuous bioactivity spread over more than 3.5 logarithmic cycles. Furthermore, the training inhibitors were selected in such a way that differences in their anti-HSL bioactivities are primarily attributable to the presence or absence of pharmacophoric features (e.g., HBA or

Table 3. Training Sets and CATALYST Run Parameters Employed for Exploring HSL Pharmacophoric Space

run no.	training set[a]	number of training compounds	selected input features: types and ranges[b]	no. of output	spacing parameter[c]
1	A	27	HBA (0−3), HBD (0−1), Hbic (0−3), RingArom (0−3)	4−5	100
2	A	27	HBA (0−3), HBD (0−1), Hbic (0−3), RingArom (0−3)	5−5	100
3	A	27	HBA (0−3), HBD (0−1), Hbic (0−3), RingArom (0−3)	4−5	300
4	A	27	HBA (0−3), HBD (0−1), Hbic (0−3), RingArom (0−3)	5−5	300
5	B	19	HBA (0−3), HBD (0−1), Hbic (0−3), RingArom (0−3)	4−5	100
6	B	19	HBA (0−3), HBD (0−1), Hbic (0−3), RingArom (0−3)	5−5	100
7	B	19	HBA (0−3), HBD (0−1), Hbic (0−3), RingArom (0−3)	4−5	300
8	B	19	HBA (0−3), HBD (0−1), Hbic (0−3), RingArom (0−3)	5−5	300
9	C	27	HBA (0−3), HBD (0−1), Hbic (0−3), RingArom (0−3)	4−5	100
10	C	27	HBA (0−3), HBD (0−1), Hbic (0−3), RingArom (0−3)	5−5	100
11	C	27	HBA (0−3), HBD (0−1), Hbic (0−3), RingArom (0−3)	4−5	300
12	C	27	HBA (0−3), HBD (0−1), Hbic (0−3), RingArom (0−3)	5−5	300
13	D	19	HBA (0−3), HBD (0−1), Hbic (0−3), RingArom (0−3)	4−5	100
14	D	19	HBA (0−3), HBD (0−1), Hbic (0−3), RingArom (0−3)	5−5	100
15	D	19	HBA (0−3), HBD (0−1), Hbic (0−3), RingArom (0−3)	4−5	300
16	D	19	HBA (0−3), HBD (0−1), Hbic (0−3), RingArom (0−3)	5−5	300

[a] The letters correspond to training sets in Table 2. [b] HBA: hydrogen bond Acceptor, HBD: hydrogen bond donor, RingArom: ring aromatic, Hbic: hydrophobic, the allowed ranges of input features are in brackets. [c] Other parameters were set to their default values.

Table 4. Performance of the Best Representatives of Clustered Pharmacophore Hypotheses Generated for HSL

training set[a]	run[b]	hypotheses[c]	pharmacophoric features in generated hypotheses	total cost	cost of null hypothesis	residual cost[d]	R[e]	F-statistic[f]	Cat.Scramble (%)
A	1	1[g]	HBA, 2×Hbic, RingArom	126.6	143.5	16.9	0.80	1.2	90
	3	1	HBA, 2×Hbic, RingArom	124.7	143.5	18.8	0.80	11.2	85
	4	1	2×HBA, 3×Hbic	124.5	143.5	19.0	0.77	2.8	95
B	5	6	2×Hbic, 2×RingArom	97.5	120.4	22.9	0.83	6.8	90
		7	HBA, 2×Hbic, RingArom	98.7	120.4	21.7	0.81	2.8	85
	7	5	HBA, 2×Hbic, RingArom	96.3	120.4	24.1	0.83	16.4	90
		8[h]	**HBA, 3×Hbic, RingArom**	**97.4**	**120.4**	**23.0**	**0.81**	**12.4**	**85**
	8	8	HBA, 3×Hbic, RingArom	98.3	120.4	22.1	0.77	0.2	95
C	9	3	HBA, 2×Hbic, RingArom	133.4	158.8	25.4	0.79	2.9	90
		4[h]	**2×HBA, Hbic, RingArom**	**133.4**	**158.8**	**25.4**	**0.78**	**14.4**	**90**
	11	1	HBA, Hbic, 2× RingArom	129.3	158.8	29.5	0.81	13.3	95
		3	HBA, Hbic, 2× RingArom	131.8	158.8	27.0	0.79	11.3	95
D	15	1	HBA, 2×Hbic, RingArom	85.4	102.5	17.1	0.90	2.8	85
	16	2	HBA, 3×Hbic, RingArom	90.0	102.5	12.5	0.74	0.5	85

[a] Correspond to training sets in Table 2. [b] Correspond to runs in Table 3. [c] Best models from their respective clusters, as judged based on F-statistic. [d] The difference between the total cost and the cost of the corresponding null hypotheses. [e] The correlation coefficients between bioactivity estimates and bioactivities of corresponding training set compounds. [f] Fischer statistic calculated based on the linear regression between the fit values of collected inhibitors (**1**−**122**, Table 1, and Figure 1) against pharmacophore hypothesis (employing the "best fit" option and eq (5)) and their respective anti-HSL bioactivities. [g] Rank of each hypothesis in each particular run by CATALYST. [h] Bolded pharmacophores emerged in the best QSAR equations (bolded).

HBD or Hbic or RingArom) rather than steric shielding and/or bioactivity-enhancing or -reducing auxiliary groups (e.g., electron donating or withdrawing groups). We gave special emphasis to the 3D diversity of the most active compounds in each training subset (Table 2) because of their significant influence on the extent of the evaluated pharmacophoric space during the constructive phase of HYPOGEN algorithm (see Section 4.1.4, Pharmacophoric Hypotheses Generation in the Experimental Section).

Guided by our reasonably restricted pharmacophore exploration concept, we restricted the software to explore pharmacophoric models incorporating from zero to one HBD feature, and from zero to three HBA, Hbic, and RingArom features instead of the default range of zero to five (Table 3). Furthermore, we instructed HYPOGEN to explore only four- and five-featured pharmacophores, i.e., ignore models of lesser number of features as shown in Table 3. The later restriction has the advantage of narrowing the investigated pharmacophoric space and representing the feature-rich nature of known HSL ligands.

In each run, the resulting binding hypotheses were automatically ranked according to their corresponding "total cost" value, which is defined as the sum of error cost, weight cost, and configuration cost (see Section 4.1.5, Assessment of the Generated Hypotheses in the Experimental Section).[17,21−25] Error cost provides the highest contribution to total cost and it is directly related to the capacity of the particular pharmacophore as 3D-QSAR model, i.e., in correlating the molecular structures to the corresponding biological responses.[17,21−25] HYPOGEN also calculates the cost of the null hypothesis, which presumes that there is no relationship in the data and that experimental activities are normally distributed about their mean. Accordingly, the greater the difference from the null hypothesis cost (residual cost, Table 4), the more likely that the hypothesis does not reflect a chance correlation.[17,21−25]

An additional validation technique, known as Cat.Scramble, was recently introduced into CATALYST.[17] This procedure is based on Fischer's randomization test.[33] In this test, the biological data and the corresponding structures are scrambled several times and the software is challenged to generate pharmacophoric models from the randomized data. The confidence in the parent hypotheses (i.e., generated from unscrambled data) is lowered proportional to the number of times the software succeeds in generating binding hypotheses from scrambled data of apparently better cost criteria than the parent hypotheses (see

Table 5. Statistical Results of the Scanned QSAR Models

model	terms[a]	$r_{(99)}$[b]	*F*-value	$r^2_{(LOO)}$[c]	$r^2_{(BS)}$[d]	$r^2_{(PRESS)}$[e]	PRESS[f]	pharmacophoric terms in QSAR model[g]
A	15	0.830	13.385	0.562	0.691	0.487	11.191	Hypo4/9
B	20	0.852	11.083	0.534	0.728	0.477	11.419	Hypo8/7, Hypo4/9
C[g]	**17**	**0.822**	**11.104**	**0.521**	**0.685**	**0.522**	**10.437**	**Hypo8/7,Hypo4/9**
D	21	0.900	16.475	0.531	0.793	0.497	10.976	Hypo8/7, Hypo4/9

[a] Number of explanatory terms including the intercept. [b] Noncross-validated correlation coefficient for 99 training compounds. [c] Cross-validation correlation coefficients determined by the leave-one-out technique. [d] Bootstrapping correlation coefficient. [e] Predictive r^2 determined for the 23 test compounds. [f] The sum of squared deviations between predicted and actual activity values for every molecule in the test set of 23 compounds. [g] This QSAR equation was selected to predict the HSL inhibitory activities of the captured hits as it yielded the best statistical criteria.

Section 4.1.5, Assessment of the Generated Hypotheses in the Experimental Section).

Eventually, 160 pharmacophore models emerged from 16 automatic HYPOGEN runs, out of which only 71 models illustrated confidence levels ≥85%. These successful models were clustered into 14 groups, and their best representatives, as judged based on their significance *F*-values (14 models, see Section 4.1.6, Clustering of the Generated Pharmacophore Hypotheses), were used in subsequent QSAR modeling (as in Table 4). Clearly, from Table 4, the representative models shared comparable features and acceptable statistical success criteria. However, their residual costs were generally less than recommended (i.e., 40),[17] as can be noticed in Table 4. This was one of the main factors that prompted us to explore the pharmacophoric space of HSL inhibitors using four training subsets and several HYPOGEN configurations.

Emergence of several statistically comparable pharmacophore models suggests the ability of HSL ligands to assume multiple pharmacophoric binding modes within the binding pocket. Therefore, it is quite challenging to select any particular pharmacophore hypothesis as a sole representative of the binding process.

2.3. QSAR Modeling. Pharmacophoric hypotheses are important tools in drug design and discovery as they provide excellent insights into ligand−macromolecule recognition and they can be used to mine for new biologically interesting scaffolds. However, their predictive value as 3D-QSAR models is usually limited by steric shielding and bioactivity-enhancing or -reducing auxiliary groups.[24] This point combined with the fact that pharmacophore modeling of HSL inhibitors furnished several binding hypotheses of comparable success criteria and mediocre residual costs (Table 4) prompted us to employ classical QSAR analysis to search for the best combination of pharmacophore(s) and other 2D descriptors capable of explaining bioactivity variation across the whole list of collected inhibitors (**1**−**122**, Table 1 and Figure 1), which should enhance the statistical significance of any QSAR-selected pharmacophore models. We employed genetic function approximation and multiple linear regression QSAR (GFA-MLR-QSAR) analysis to search for an optimal QSAR equation(s).

GFA-MLR-QSAR selects optimal descriptor combinations based on the Darwinian concept of genetic evolution whereby the statistical criteria of regression models from different descriptor combinations (chromosomes) are employed as fitness criteria.[17] GFA-MLR-QSAR analysis was employed to explore various combinations of pharmacophores and other structural descriptors and to evaluate their statistical properties as predictive QSAR models.

The fit values obtained by mapping the 14 representative hypotheses against all collected HSL inhibitors (**1**−**122**, Table 1 and Figure 1) were enrolled as independent variables (genes) in a cycle of GFA-MLR-QSAR analysis over 30000 iterations employing Friedman's LOF fitness criterion (see Section 4.1.7, QSAR Modeling in the Experimental Section).[34,35] However, because it is essential to access the predictive power of the resulting QSAR models on an external set of inhibitors, we randomly selected 23 molecules (marked with footnote *a* in Table 1, see Section 4.1.7, QSAR Modeling in the Experimental Section) and employed them as external test molecules for validating the QSAR models (r^2_{PRESS}). Moreover, all QSAR models were cross-validated automatically using the leave-one-out cross-validation in CERIUS2.[34,35]

Table 5 shows the statistical criteria of the resulting top-ranking QSAR models. Surprisingly, the optimal QSAR (model C in Table 5) required the pharmacophore fit values to be in quadratic forms to access significant extrapolatory prediction against the external test set. Equation 1 shows the details of the optimal QSAR model. Figure 2 shows the corresponding scatter plots of experimental versus estimated bioactivities for the training and testing inhibitors.

$$\log(1/IC_{50}) = 4.97 + 9.53\times10^{-3}(\text{Hypo8/7})^2 + 27.50\times10^{-3}(\text{Hypo4/9})^2 - 1.00\times10^{-6}(\text{JursPNSA2})^2 - 0.74(\text{AtypeN68})^2 - 0.43(\text{AtypeN72})^2 - 1.24(\text{AtypeN74})^2 - 2.38\times10^{-2}(\text{AtypeH51})^2 - 3.28(\text{AtypeC41})^2 - 0.40(\text{AtypeC8})^2 - 18.67\times10^{-3}(\text{SssO})^2 - 5.85\times10^{-3}(\text{SsCH3})^2 - 11.02\times10^{-3}(\text{SsOH})^2 - 0.15(\text{SssNH})^2 - 0.25(\text{SaaaC})^2 - 2.08\times10^{-2}(\text{Shadow}-\textit{Y}\text{length})^2 - 0.17(\text{Shadow}-\text{nu})^2$$
$$r_{99} = 0.82, F\text{-statistic} = 11.10, r^2_{BS} = 0.69, r^2_{LOO} = 0.52, r^2_{PRESS(23)} = 0.52 \quad (1)$$

where r_{99} is the correlation coefficient against 99 training compounds, r^2_{LOO} is the leave-one-out correlation coefficient, r^2_{BS} is the bootstrapping regression coefficient, and r^2_{PRESS} is the predictive r^2 determined for the 23 test compounds.[34,35] Hypo8/7 and Hypo4/9 represent the fit values of the training compounds against these two pharmacophores as calculated from eq 5 (see Section 4.1.5, Assessment of the Generated Hypotheses). JursPNSA2 is the total charge weighted partial negatively charged molecular surface area (obtained by multiplying the partial negative solvent-accessible surface area by the total negative charge). AtypeN68, AtypeN72, AtypeN74, AtypeH51, AtypeC8, and AtypeC41 are atom-type-based AlogP descriptors. SsOH, SssO, SsCH3, SssNH, and SaaaC are the electrotopological sum descriptors for hydroxyl, ether oxygen, methyl, secondary amine, and aromatic carbons, respectively. Shadow descriptors are geometric descriptors that characterize the shape of the molecules; Shadow−*Y*length represents the length of molecule in the *Y* dimension, while Shadow−nu represents the ratio between the largest to smallest dimensions in a molecule.[34]

The emergence of two orthogonal pharmacophoric models (Hypo8/7 and Hypo4/9, cross-correlation $r^2 = 0.54$) in eq 1 suggests that they represent two complementary binding modes accessible to ligands within the binding pocket of HSL, which means that one of the pharmacophores can optimally explain the bioactivities of some training inhibitors, while the other explains the remaining inhibitors. Similar conclusions were reached about the binding pockets of other targets, e.g., factor

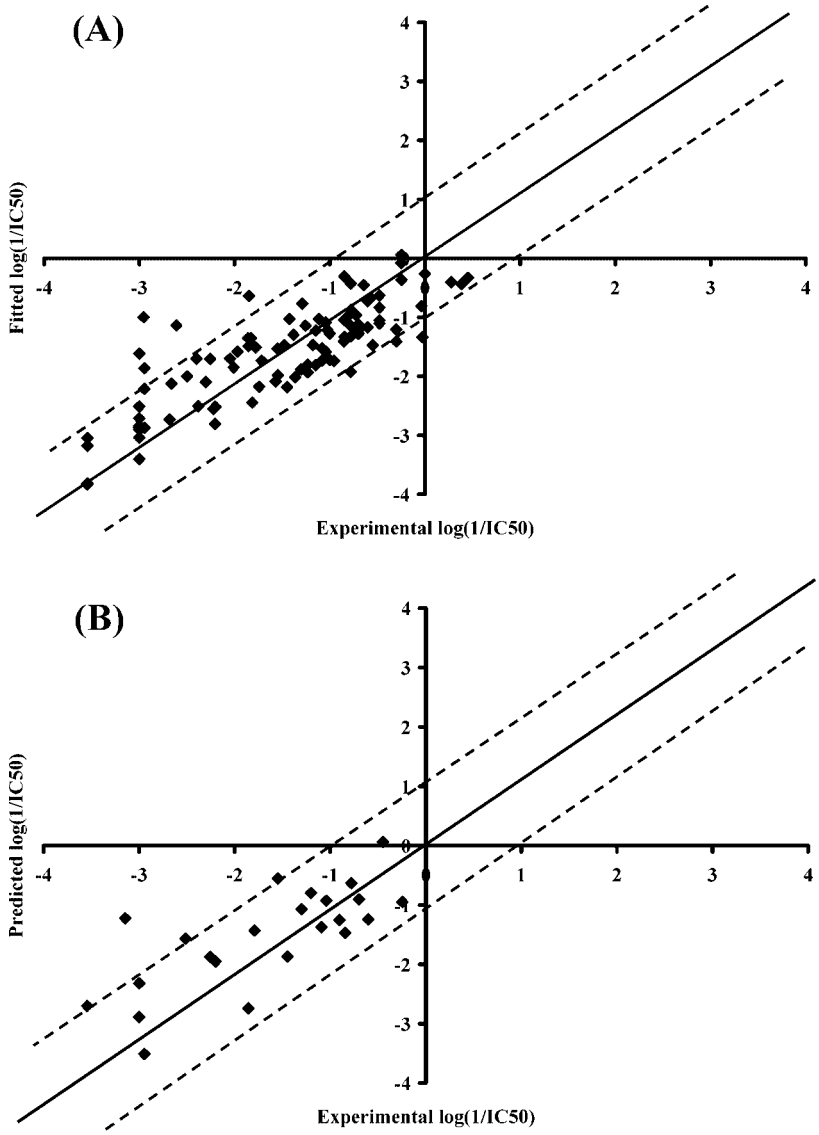

Figure 2. Experimental versus (A) fitted (99 compounds, $r^2_{LOO} = 0.521$) and (B) predicted (23 compounds, $r^2_{PRESS} = 0.522$) bioactivities (expressed in nM concentrations) calculated from the best QSAR model eq 1. The solid lines are the regression lines for the fitted and predicted bioactivities of training and test compounds, respectively, whereas the dotted lines indicate the 1.0 log point error margins.

Xa, GSK-3β, and Mur F, based on the emergence of several orthogonal binding pharmacophores in the corresponding optimal QSAR models.[27−29]

Figures 3 and 4 show Hypo4/9 and Hypo8/7 and how they map training compound **115** (IC_{50} = 1.09 nM) and the most potent hit compound **123** (IC_{50} = 0.214 μM, see below), while Table 6 shows the *X*, *Y*, and *Z* coordinates of the two pharmacophores.

Emergence of the two Pharmacophore models in quadratic format in eq 1 suggests that ligand/HSL affinity is more sensitive to fitting the pharmacophoric models at higher fit values compared to lower values, i.e., misalignment among the attracting moieties within the complex drastically reduce ligand/HSL affinities, suggesting that ligand binding to HSL is extremely sensitive to minor misalignments between attracting moieties within the complex.

Emergence of electrotopological and Shadow descriptors in eq 1 illustrate a certain role played by the ligands' topology in the binding process. However, despite their predictive significance, their information content is quite obscure. Nevertheless, emergence of JursPNSA2 in eq 1 associated with a negative regression coefficient suggests an inverse relationship between ligand/HSL affinity and the ligands' negative charges. We believe this trend is explainable by the fact that ionic groups favor hydration over docking into the binding site.

2.4. Addition of Exclusion Volumes. Although ligand-based pharmacophores serve as excellent tools to probe ligand/macromolecule recognition and as useful 3D QSAR models and search queries, they lack steric constrains necessary to define the size of the binding pocket. This liability renders pharmacophoric models rather promiscuous. Therefore, we decided to complement our QSAR-selected pharmacophores with exclusion spheres employing the HipHop-REFINE module implemented within CATALYST.[17] Excluded volumes resemble sterically inaccessible regions within the binding site (see Section 4.1.8, Addition of Exclusion Volumes in the Experimental Section).[17,36] The fact that the optimal QSAR model (eq 1) revealed two orthogonal pharmacophoric models, indicative of at least two distinct binding modes, prompted us to carefully select two structurally diverse training subsets for HipHop-REFINE modeling, E and F, to add exclusion spheres for Hypo8/7 and Hypo4/9, respectively (Tables 7 and 8). The training compounds were selected in such a way that the bioactivities of weakly active

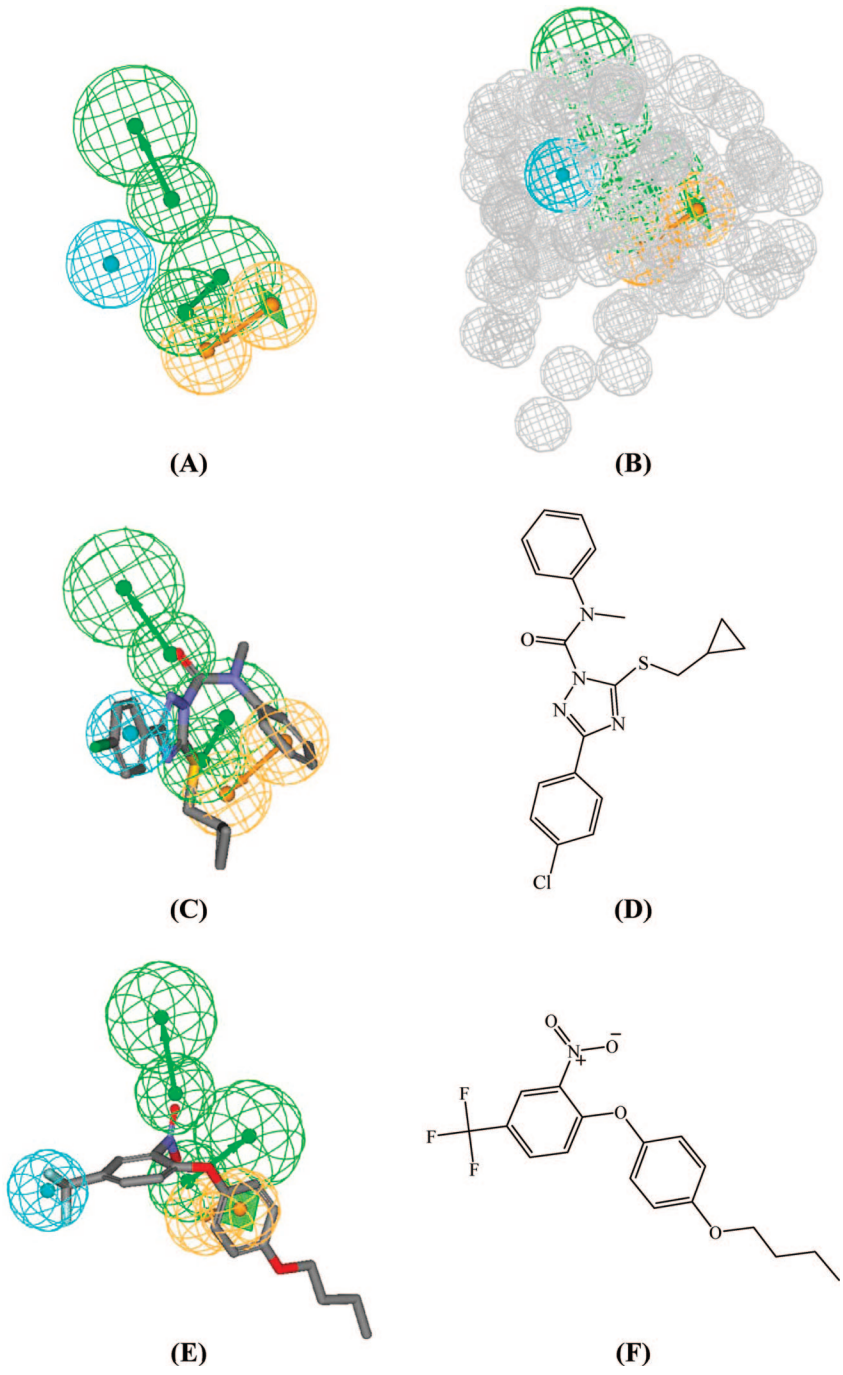

Figure 3. Hypo4/9. (A) Pharmacophoric features of the binding model: HBA as green vectored spheres, Hbic as blue spheres, and RingArom as orange vectored spheres; (B) Hypo4/9 with exclusion volumes (gray spheres); (C) Hypo4/9 fitted against **115** (Table 1 and Figure 1, $IC_{50} = 1.09$ nM); (D) The chemical structures of compound **115**; (E) Hypo4/9 fitted against the hit **123** (Table 9, $IC_{50} = 0.214$ μM); (F) The chemical structure of **123**.

compounds are explainable by steric clashes with the binding pocket. Figures 3b and 4b show sterically refined versions of Hypo4/9 (78 added exclusion volumes) and Hypo8/7 (99 added exclusion volumes), respectively.

2.5. In Silico Screening and Subsequent in Vitro Evaluation. The proposition that Hypo8/7 and Hypo4/9 are complementary, and therefore represent different binding modes within the binding pocket, prompted us to employ their sterically refined versions (i.e., with exclusion volumes, Figures 3 and 4) as 3D search queries against two available 3D flexible structural databases, namely the NCI list of compounds (238819 compounds) and our *in-house* built database of known drugs and agrochemicals (2602 compounds). Collectively, Hypo4/9 and Hypo8/7 captured 9608 hit compounds. Hits are defined as those compounds that have their chemical groups spatially overlap (map) with corresponding features within the particular pharmacophoric model. Hypo4/9 captured 2523 hits from both databases: 2506 hits from the NCI and 17 hits from the drugs and agrochemicals list. NCI hits (2506) were subsequently filtered based on Lipinski's and Veber's rules,[37,38] leaving a reduced list of 2354 compounds. On the other hand, Hypo8/7 captured 7085 compounds from both databases: 6957 hits from the NCI database and 128 hits from our drugs and agrochemicals list. Again, the NCI list of hits (6957) was shortened to 5910 compounds based on Lipinski's and Veber's rules. Captured

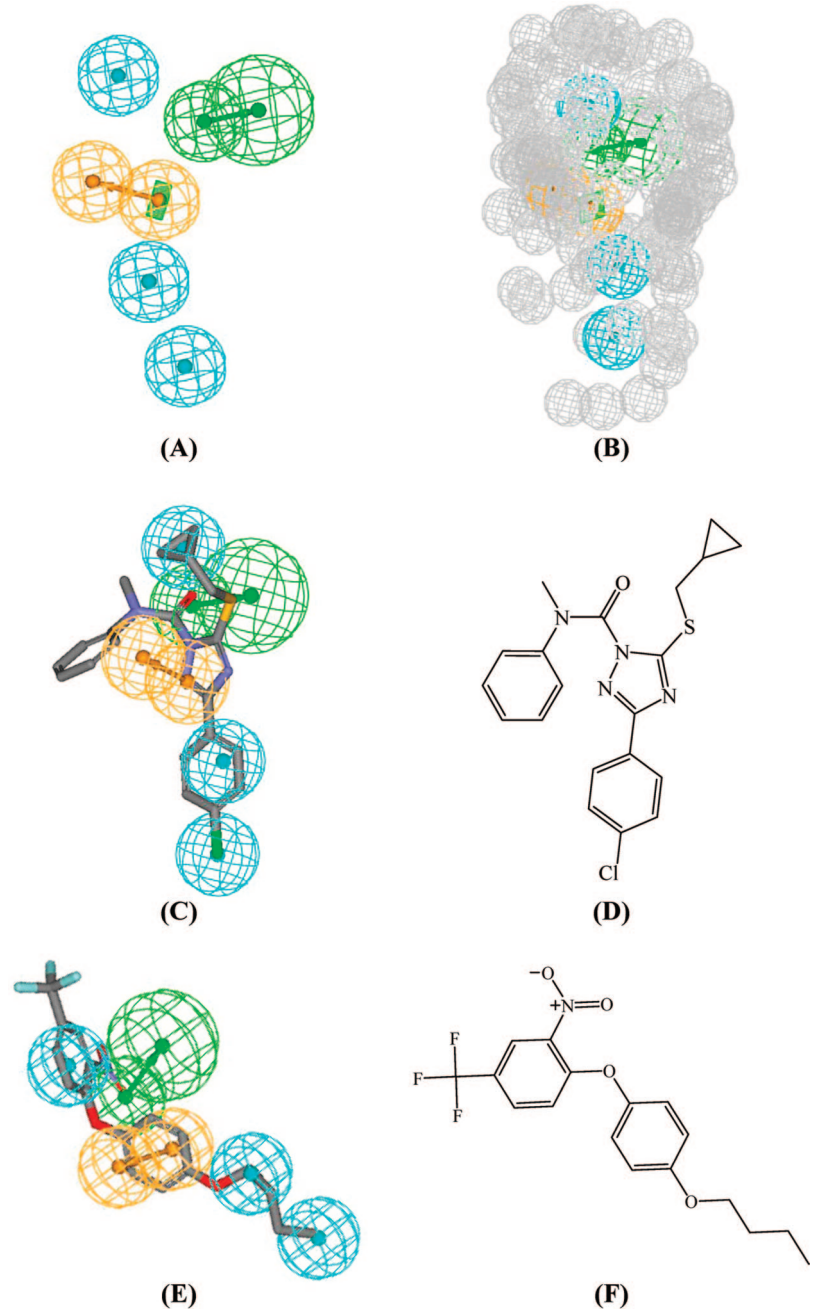

Figure 4. Hypo8/7. (A) The pharmacophoric features of the binding model: HBA as green vectored spheres, Hbic as blue spheres, and RingArom as orange vectored spheres; (B) Hypo8/7 with exclusion volumes (gray spheres); (C) Hypo8/7 fitted against **115** (Table 1 and Figure 1, $IC_{50} = 1.09$ nM); (D) The chemical structures of compound **115**; (E) Hypo8/7 fitted against the hit **123** (Table 9, $IC_{50} = 0.214$ μM); (F) The chemical structure of **123**.

hits from our drug and agrochemical list of compounds were left without postfiltration by Lipinski's or Veber's rules.

The remaining hits were fitted against Hypo4/9 and Hypo8/7 (without exclusion volumes), and their fit values were substituted in QSAR eq 1 to determine their predicted bioactivities. The highest-ranking available hits (61 compounds, either purchased commercially or provided kindly from the NCI) were evaluated in vitro against HSL at 1 or 10 μM concentrations. However, 37 compounds were found to be active HSL inhibitors. Figure 5 and Table 9 show the active hits and their corresponding estimated and experimental anti-HSL bioactivities. Hits of inhibitory percentages $\geq$50% were further tested to determine their IC_{50} values against HSL. Interestingly, their corresponding dose/response regression lines illustrated excellent correlation coefficients, strongly suggestive of nonpromiscuous inhibitory behavior.

Clearly, from Figure 5 and Table 9, our active hits emphasized diphenyl ethers as promising anti-HSL scaffold for subsequent optimization. Although the HSL inhibitory potential of this scaffold was recently highlighted,[11] our active hits undermined the previous belief that active HSL inhibitors should include covalent-bond forming groups, e.g., carbamate.[7,10,12−16] This conclusion is particularly evident in compounds **123**, **125**, **133**, **148** (bifenox), **149**, **150**, **151**, and **152** as well as in the related isosteres **155** and **159**. The herbicidal agent bifenox ($IC_{50} =$ 0.43 μM) and the nonsteroidal anti-inflammatory naproxen (**157**,

Table 6. Pharmacophoric Features and Corresponding Weights, Tolerances, and 3D Coordinates of Hypo8/7[a] and Hypo4/9[b]

			chemical features						
model	definitions		HBA		Hbic	Hbic	Hbic	RingArom	
Hypo8/7[a]	weights		2.39102		2.39102	2.39102	2.39102	2.39102	
	tolerances		1.60	2.20	1.60	1.60	1.60	1.60	1.60
	coordinates	*X*	0.29	−0.91	−3.94	0.04	−3.54	−1.15	−0.26
		Y	1.10	1.73	−7.45	3.61	−3.84	−1.40	−0.58
		Z	2.84	5.52	0.97	−0.01	0.28	0.72	−2.03

model	definitions		HBA		HBA		Hbic	RingArom	
Hypo4/9[b]	weights		2.07464		2.07464		2.07464	2.07464	
	tolerances		1.60	2.20	1.60	2.20	1.60	1.60	1.60
	coordinates	*X*	−0.88	−0.63	2.97	5.66	2.70	−1.61	−2.42
		Y	−2.03	−4.77	−2.60	−3.95	3.64	−1.34	−1.94
		Z	−1.02	0.27	−0.07	−0.48	−2.18	1.99	−0.83

[a] Hypo8/7 is hypothesis number 8 generated in run number 7. [b] Hypo4/9 is hypothesis number 4 generated in run number 9.

Table 7. Training Subset E Used for Adding Excluded Spheres for Hypo8/7 Using HIPHOP-REFINE Module of CATALYST

compd[a]	IC_{50} (nM)	principal value	MaxOmitFeat[b]	compd[b]	IC_{50} (nM)	principal value	MaxOmitFeat[b]
17	4.00	2	0	**52**	52	0	1
63	1.00	2	0	**54**	62	0	1
64	3.00	2	0	**55**	900	0	1
66	3.00	2	0	**56**	93	0	1
92	0.353	2	0	**59**	180	0	1
93	3.71	2	0	**68**	102	0	1
94	1.06	2	0	**76**	37	0	1
95	0.53	2	0	**77**	160	0	1
98	1.76	2	0	**78**	480	0	1
100	1.76	2	0	**79**	250	0	1
109	1.76	2	0	**83**	>1000	0	1
111	3.53	2	0	**85**	>1000	0	1
113	2.82	2	0	**87**	460	0	1
114	3.00	2	0	**89**	326	0	1
115	1.09	2	0	**90**	>1000	0	1
117	1.76	2	0	**91**	>1000	0	1
13	71.00	0	1	**103**	882.35	0	1
20	>1000	0	1	**105**	158.82	0	1
21	>1000	0	1	**108**	158.82	0	1
22	N/A[c]	0	1	**15**	55	0	2
28	111	0	1	**32**	>1000	0	2
29	408	0	1	**34**	N/A[c]	0	2
33	180	0	1	**35**	>1000	0	2
38	240	0	1	**39**	1400	0	2
43	72	0	1	**40**	N/A[c]	0	2
44	>1000	0	1	**42**	N/A[c]	0	2
45	60	0	1	**46**	>1000	0	2
47	314	0	1	**81**	166	0	2
48	65	0	1	**82**	200	0	2
51	67	0	1	**86**	N/A[c]	0	2

[a] Compounds' numbers are as in Table 1 and Figure 1. [b] MaxOmitFeat: maximum omitted features. [c] N/A: not active.

IC_{50} = 1.20 μM) are particularly interesting due to their favorable toxicity profiles[39] and therefore can serve as excellent starting leads for subsequent optimization.

It must be remembered that, although we employed rat HSL to validate our hits, there is significant homology between rat and human HSL (83% identity) to robustly conclude the validity of our hits against human HSL.[40]

3. Conclusion

HSL inhibitors are currently considered as potential treatments for diabetes and obesity. The pharmacophoric space of HSL inhibitors was explored via four diverse sets of inhibitors and using CATALYST-HYPOGEN to identify high quality binding model(s). Subsequently, genetic algorithm and multiple linear regression analysis were employed to access optimal QSAR model capable of explaining anti-HSL bioactivity variation across 122 collected HSL inhibitors (r = 0.822, F = 11.104, r^2_{LOO} = 0.521, r^2_{PRESS} against 23 external test inhibitors = 0.522). Two pharmacophoric models emerged in the QSAR equation, suggesting the existence of at least two distinct binding modes accessible to ligands within HSL binding pocket.

The QSAR equation and the associated pharmacophoric models were experimentally validated by the identification of several potent HSL inhibitors retrieved via in silico mining of two structural databases, namely the NCI list of compounds and our *in-house* built structural database of established drugs and agrochemicals. One of the potent inhibitors is the herbicidal agent bifenox (**148**, IC_{50} = 0.43 μM). Our results suggest that the combination of pharmacophoric exploration and QSAR analyses can be useful tool for finding new HSL inhibitors.

4. Experimental Section

4.1. Molecular Modeling. 4.1.1. Software and Hardware. The following software packages were utilized in the present research: (1) CATALYST (Version 4.11), Accelrys Inc. (www.ac-

Table 8. Training Subset F Used for Adding Excluded Spheres for Hypo4/9 Using HIPHOP-REFINE Module of CATALYST

compd[a]	IC_{50} (nM)	principal value	MaxOmitFeat[b]	compd[a]	IC_{50} (nM)	principal value	MaxOmitFeat[b]
113	2.82	2	0	**82**	200	0	1
114	3.00	2	0	**83**	>1000	0	1
115	1.09	2	0	**85**	>1000	0	1
116	7.06	2	0	**86**	N/A[c]	0	1
117	1.76	2	0	**87**	460	0	1
118	12.35	2	0	**89**	326	0	1
119	4.41	2	0	**90**	>1000	0	1
120	5.29	2	0	**91**	>1000	0	1
13	71	0	1	**97**	882.35	0	1
15	55	0	1	**103**	882.35	0	1
22	N/A[c]	0	1	**107**	70.59	0	1
29	408	0	1	**108**	158.82	0	1
32	>1000	0	1	**112**	882.35	0	1
33	180	0	1	**10**	14.00	0	2
34	N/A[c]	0	1	**12**	11.00	0	2
25	>1000	0	1	**20**	>1000	0	2
44	>1000	0	1	**21**	>1000	0	2
45	60	0	1	**28**	111	0	2
48	>65	0	1	**38**	240	0	2
51	67	0	1	**39**	1400	0	2
52	52	0	1	**40**	N/A[c]	0	2
54	62	0	1	**41**	15	0	2
60	>1000	0	1	**42**	N/A[c]	0	2
68	102	0	1	**43**	72	0	2
76	37	0	1	**46**	>1000	0	2
77	160	0	1	**47**	314	0	2
78	480	0	1	**55**	900	0	2
79	250	0	1	**56**	93	0	2
81	166	0	1	**59**	180	0	2

[a] Compounds' numbers are as in Table 1 and Figure 1. [b] MaxOmitFeat: Maximum omitted features. [c] N/A: not active.

celrys.com), USA; (2) CERIUS2 (Version 4.10), Accelrys Inc. (www.accelrys.com), USA; (3) CS ChemDraw Ultra 6.0, Cambridge Soft Corp. (http:// www.cambridgesoft.Com), USA. Pharmacophore and QSAR modeling studies were performed using CATALYST (HYPOGEN module) and CERIUS2 software suites from Accelrys Inc. (San Diego, California, www.accelrys.com) installed on a Silicon Graphics Octane2 desktop workstation equipped with a dual 600 MHz MIPS R14000 processor (1.0 GB RAM) running the Irix 6.5 operating system. Structure drawing was performed employing ChemDraw Ultra 6.0, which was installed on a Pentium 4 PC.

4.1.2. Data Set. The structures of 122 HSL inhibitors (**1**−**122**, Table 1, Figure 1) were collected from recently published literature.[7,10] Although the in vitro bioactivities of the collected inhibitors were gathered from two separate articles and were determined employing two bioassay methodologies, it was possible to normalize their anti-HSL bioactivities based on the fact that compound **59** was bioassayed by both methods. The bioactivities were expressed as the concentrations of the test compounds that inhibited the activity of HSL by 50% (IC_{50}, nM). The logarithm of measured IC_{50} (nM) values were used in the three-dimensional quantitative structure activity analysis (3D-QSAR), thus correlating the data linear to the free energy change.

In a few cases where the IC_{50} values of some compounds were expressed as being higher than 1000 nM (e.g., **20**, **21**, **32**, **35**, **44**, **46**, **60**, **83**, **85**, **90**, and **91**), we assumed that their IC_{50} values to be equal to 1000 nM. Similarly, if a particular compound was reported to be devoid of activity, we assumed it IC_{50} value to be equal to 3500 nM (4 logarithmic cycles away from the most potent inhibitor, e.g., **22**, **34**, **40**, **42**, and **86**). These assumptions are necessary to allow pharmacophore modeling, statistical correlation, and QSAR analysis. The logarithmic transformation of IC_{50} values should minimize any potential errors resulting from such assumptions.

The two-dimensional (2D) chemical structures of the inhibitors were sketched using ChemDraw Ultra and saved in MDL-molfile format. Subsequently, they were imported into CATALYST, converted into corresponding standard 3D structures, and energy minimized to the closest local minimum using the molecular mechanics CHARMm force field implemented in CATALYST. The resulting 3D structures were utilized as starting conformers for CATALYST conformational analysis.

4.1.3. Conformational Analysis. The molecular flexibilities of the collected compounds were taken into account by considering each compound as a collection of conformers representing different areas of the conformational space accessible to the molecule within a given energy range. Accordingly, the conformational space of each inhibitor (**1**−**122**, Figure 1 and Table 1) was explored by adopting the "best conformer generation" option within CATALYST based on the generalized CHARMm force field implemented in the program. Default parameters were employed in the conformation generation procedure, i.e., a conformational ensemble was generated with an energy threshold of 20 kcal/mol from the local minimized structure, which has the lowest energy level and a maximum limit of 250 conformers per molecule. This search procedure will probably identify the best three-dimensional arrangement of chemical functionalities, explaining the activity variations among the training set.[17]

4.1.4. Pharmacophoric Hypotheses Generation. All 122 molecules with their associated conformational models were regrouped into a spreadsheet. The biological data of the inhibitors were reported with an "uncertainty" value of 3, which means that the actual bioactivity of a particular inhibitor is assumed to be situated somewhere in an interval ranging from one-third to three times the reported bioactivity value of that inhibitor.[21,23,25] Subsequently, four structurally diverse training subsets: sets A, B, C, and D in Table 2, respectively, were carefully selected from the collection for pharmacophore modeling. Typically, CATALYST requires informative training sets that include at least 16 compounds of evenly spread bioactivities over at least three-and-a-half logarithmic cycles. Lesser training lists could lead to chance correlation and thus faulty models.[21,23,25]

The selected training sets were utilized to conduct 16 modeling runs to explore the pharmacophoric space of HSL inhibitors (Table 3). The exploration process included altering interfeature spacing parameter (100 and 300 picometers) and the maximum number of allowed features in the resulting pharmacophore hypotheses, i.e., they were allowed to vary from 4 to 5 for the first and the third

Table 9. Hit Molecules Captured by Hypo8/7 and Hypo4/9 and Their Corresponding QSAR Estimates from eq *6* and Their in Vitro Bioactivities

		fit values against[b]		QSAR estimates[c]		actual affinities[d]	
hit compd[a]	name or NCI code	Hypo8/7	Hypo4/9	log(1/IC_{50})	IC_{50} (nM)	% inhibition at 1 or 10 μM	IC_{50} (μM)
123	NCI 58425	11.22	7.20	1.85	0.014	64[e]	0.21 (0.99[g])
124	NCI 86895	10.54	5.45	0.94	0.114	15[f]	
125	NCI 107527	10.92	7.33	0.60	0.250	31[f]	
126	NCI 109483	9.71	6.47	−1.07	11.770	24[f]	
127	NCI 133699	10.66	7.63	1.30	0.050	52[f]	5.00 (0.90[g])
128	NCI 139606	8.70	7.59	1.19	0.065	15[e]	
129	NCI 159878	9.70	7.80	−1.17	14.64	45[e]	2.98 (0.94[g])
130	NCI 165451	6.89	5.91	0.29	0.513	2[f]	
131	NCI 177967	10.32	7.45	0.36	0.433	29[f]	
132	NCI 268685	5.09	7.47	2.00	0.010	67[e]	0.51 (0.76[g])
133	NCI 282461	9.57	7.60	0.73	0.187	30[f]	
134	NCI 293836	10.70	6.25	0.09	0.805	24[e]	
135	NCI 343540	10.10	7.00	1.66	0.022	24[f]	
136	NCI 608052	8.32	8.02	1.47	0.034	26[f]	
137	NCI 675782	9.53	7.08	−0.54	3.500	27[e]	
138	NCI 16296	0	5.08	1.37	0.043	9[e]	
139	NCI 16962	0	6.76	1.23	0.059	12[e]	
140	NCI 21442	0	7.18	1.12	0.076	21[e]	
141	NCI 23869	0	4.73	1.04	0.092	12[f]	
142	NCI 23872	0	4.70	1.16	0.069	24[f]	
143	NCI 203307	3.21	4.74	1.40	0.040	3[f]	
144	NCI 57653	0	4.08	0.77	0.170	23[e]	
145	NCI 80427	0	5.56	1.25	0.056	14[f]	
146	NCI 117769	0	6.22	0.91	0.122	23[f]	
147	NCI 177999	10.16	0.94	1.41	0.039	10[f]	
148	bifenox	10.63	4.08	1.84	0.015	60[e]	0.43 (0.98[g])
149	chlorfenson	3.38	7.57	3.15	0.001	26[f]	
150	esfenvalerate	8.43	7.18	−1.04	10.900	33[e]	
151	fenvalerate	7.79	6.81	−0.76	5.690	37[e]	
152	fenpropathrin	7.69	6.61	−1.18	14.990	35[e]	
153	ethiofencarb	9.10	5.33	−0.94	8.660	52[f]	0.37 (0.99[g])
154	silafluofen	10.95	1.73	0.02	0.950	6[e]	
155	oxybenzone[h]	3.22	6.62	2.30	0.005	44[f]	3.25 (0.98[g])
156	capsaicin	6.53	3.55	−0.68	4.780	33[f]	
157	naproxen	8.88	0	1.28	0.053	64[f]	1.20 (0.99[g])
158	dibenzoylmethane	0	5.15	2.40	0.004	28[f]	
159	benzyl benzoate	0	3.92	1.64	0.023	66[f]	1.10 (0.96[g])

[a] Hits shown in Figure 5. [b] Best-fit values against each binding hypothesis calculated by eq 5. [c] QSAR estimates from eq 1. [d] In vitro enzyme inhibition. Each value (percent inhibition or IC_{50}) represents the average of at least three measurements. [e] % Inhibition at 1 μM inhibitor concentration. [f] % Inhibition at 10 μM inhibitor concnetration. [g] This value represents the correlation coefficient of the corresponding dose−response line at three concentrations. [h] Oxybenzone: 2-hydroxy-4-methoxybenzophenone.

runs and from 5 to 5 for the second and the fourth runs for each training set, as shown in Table 3.

Pharmacophore modeling employing CATALYST proceeds through three successive phases: the constructive phase, subtractive phase, and optimization phase.[21,23,25] During the constructive phase, CATALYST generates common conformational alignments among the most-active training compounds. Only molecular alignments based on a maximum of five chemical features are considered. The program identifies a particular compound as being within the most active category if it satisfies eq 2.[21,23,25]

$$(\mathrm{MAct} \times \mathrm{UncMAct}) - (\mathrm{Act}/\mathrm{UncAct}) > 0.0 \qquad (2)$$

where "MAct" is the activity of the most active compound in the training set, "Unc" is the uncertainty of the compounds, and "Act" is the activity of the training compounds under question. However, if there are more than eight most-active inhibitors, only the top eight are used.

In the subsequent subtractive phase, CATALYST eliminates some hypotheses that fit inactive training compounds. A particular training compound is defined as being inactive if it satisfies eq 3:[21,23,25]

$$\log(\mathrm{Act}) - \log(\mathrm{MAct}) > 3.5 \qquad (3)$$

However, in the optimization phase, CATALYST applies fine perturbations in the form of vectored feature rotation, adding new feature and/or removing a feature, to selected hypotheses that survived the subtractive phase, in an attempt to find new models of enhanced bioactivity/mapping correlation, i.e., improved 3D-QSAR properties.

Table 2 shows the most active, least active, and intermediately active compounds of each training subset as categorized by eqs 2 and 3.

Eventually, CATALYST selects the highest-ranking models (10 by default) and presents them as the optimal pharmacophore hypotheses resulting from the particular automatic modeling run. Our pharmacophore exploration efforts (16 automatic runs, Tables 2 and 3) culminated in 160 pharmacophore models of variable qualities.

4.1.5. Assessment of the Generated Hypotheses. When generating hypotheses, CATALYST attempts to minimize a cost function consisting of three terms: weight cost, error cost, and configuration cost.[17,21−25] Weight cost is a value that increases as the feature weight in a model deviates from an ideal value of 2. The deviation between the estimated activities of the training set and their experimentally determined values adds to the error cost. The activity of any compound can be estimated from a particular hypothesis through eq 4:[17]

$$\log(\text{Estimated Activity}) = I + \mathrm{Fit} \qquad (4)$$

where I = the intercept of the regression line obtained by plotting the log of the biological activity of the training set compounds against the Fit values of the training compounds. The Fit value for any compound is obtained automatically employing eq 5:[17]

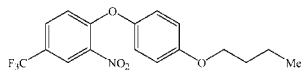

123

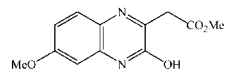

124

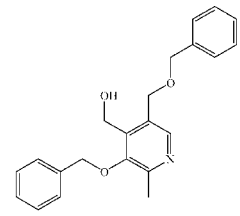

125

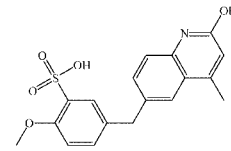

126

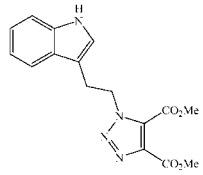

127

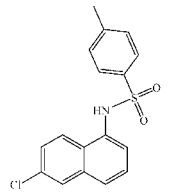

128

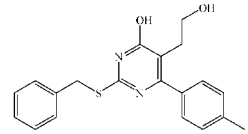

129

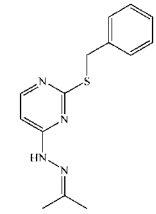

130

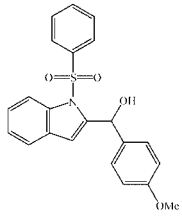

131

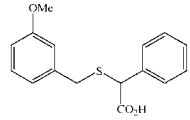

132

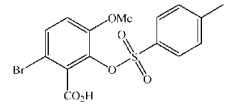

133

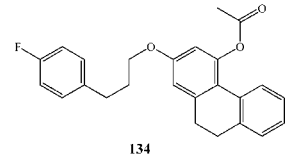

134

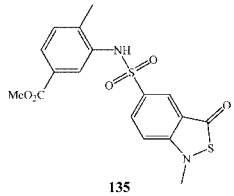

135

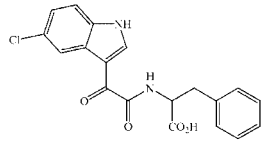

136

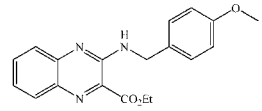

137

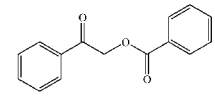

138

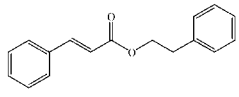

139

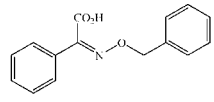

140

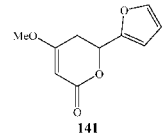

141

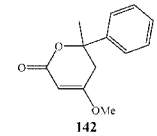

142

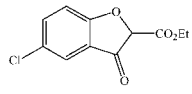

143

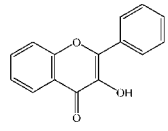

144

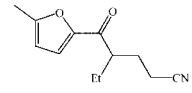

145

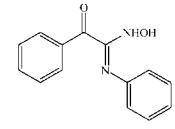

146

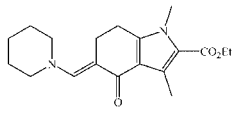

147

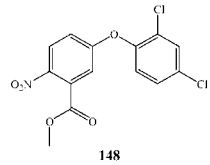

148

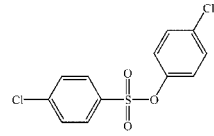

149

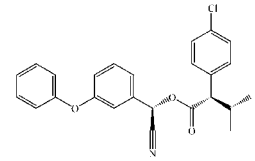

150

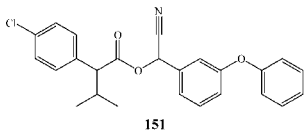

151

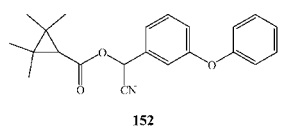

152

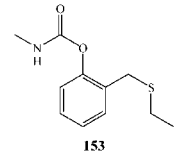

153

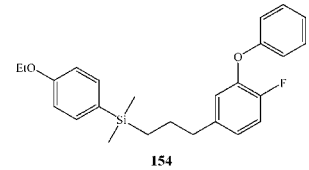

154

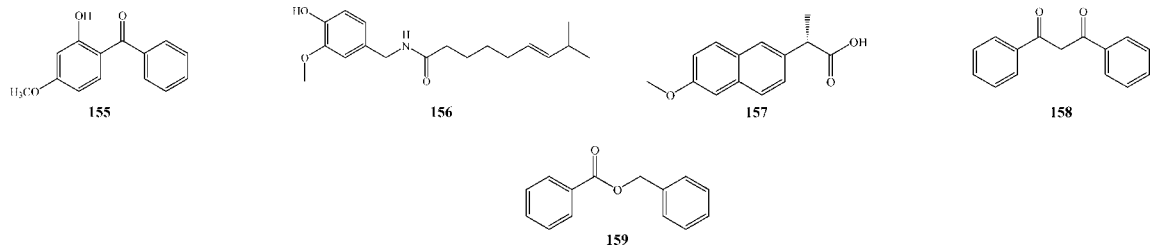

Figure 5. Chemical structures of the tested highest-ranking hits (as suggested by the best QSAR model, eq 1).

$$\text{Fit} = \sum\text{mapped hypothesis features} \times W[1 - \sum(\text{disp}/\text{tol})^2] \quad (5)$$

where ∑mapped hypothesis features represents the number of pharmacophore features that successfully superimpose (i.e., map or overlap with) corresponding chemical moieties within the fitted compound, *W* is the weight of the corresponding hypothesis feature spheres. This value is fixed to 1.0 in CATALYST-generated models. disp is the distance between the center of a particular pharmacophoric sphere (feature centroid) and the center of the corresponding superimposed chemical moiety of the fitted compound; tol is the radius of the pharmacophoric feature sphere (known as Tolerance, equal to 1.6 Å by default). $\sum(\text{disp}/\text{tol})^2$ is the summation of $(\text{disp}/\text{tol})^2$ values for all pharmacophoric features that successfully superimpose corresponding chemical functionalities in the fitted compound.[17]

The third term, i.e., the configuration cost, penalizes the complexity of the hypothesis. This is a fixed cost, which is equal to the entropy of the hypothesis space. The more the numbers of features (a maximum of five) in a generated hypothesis, the higher is the entropy with subsequent increase in this cost. The overall cost (total cost) of a hypothesis is calculated by summing over the three cost factors. However, error cost is the main contributor to total cost.

CATALYST also calculates the cost of the null hypothesis, which presumes that there is no relationship in the data and that experimental activities are normally distributed about their mean. Accordingly, the greater the difference from the null hypothesis cost, the more likely that the hypothesis does not reflect a chance correlation. In a successful automatic modeling run, CATALYST ranks the generated models according to their total costs.[17]

An additional approach to assess the quality of CATALYST-HYPOGEN pharmacophores is to cross-validate them using the Cat.Scramble program implemented in CATALYST. This validation procedure is based on Fischer's randomization test.[33] In this validation test, we selected a 95% confidence level, which instructs CATALYST to generate 19 random spreadsheets by the Cat.Scramble command. Subsequently, CATALYST-HYPOGEN is challenged to use these random spreadsheets to generate hypotheses using exactly the same features and parameters used in generating the initial unscrambled hypotheses.[41] Success in generating pharmacophores of comparable cost criteria to those produced by the original unscrambled data reduces the confidence in the training compounds and the unscrambled original pharmacophore models. On the basis of Fischer randomization criteria, only 71 pharmacophores exceeded the 85% significance threshold for subsequent processing (clustering and QSAR analyses).

4.1.6. Clustering of the Generated Pharmacophore Hypotheses. The successful models (71) were clustered into 14 groups utilizing the hierarchical average linkage method available in CATALYST. Subsequently, the highest-ranking representatives, as judged based on their significance *F*-values, were selected to represent their corresponding clusters in subsequent QSAR modeling. Table 4 shows information about representative pharmacophores including their pharmacophoric features, success criteria, and differences from corresponding null hypotheses. The table also shows the corresponding Cat.Scramble confidence levels for each representative pharmacophore.

4.1.7. QSAR Modeling. A subset of 99 compounds from the total list of inhibitors (**1**−**122**, Table 1 and Figure 1) was utilized as a training set for QSAR modeling. However, because it is essential to access the predictive power of the resulting QSAR models on an external set of inhibitors, the remaining 23 molecules (ca. 20% of the data set) were employed as an external test subset for validating the QSAR models. The test molecules were selected as follows: the 122 inhibitors were ranked according to their IC_{50} values, and then every fifth compound was selected for the test set starting from the high-potency end. This selection considers the fact that the test molecules must represent a range of biological activities similar to that of the training set. The selected test inhibitors are: **3**, **4**, **12**, **20**, **23**, **30**, **36**, **39**, **53**, **54**, **57**, **59**, **60**, **61**, **86**, **89**, **98**, **99**, **104**, **105**, **106**, **113**, and **118** (marked with footnote [a] in Table 1, Figure 1).

The logarithm of measured $1/IC_{50}$ (nM) values were used in QSAR, thus correlating the data linear to the free energy change. The chemical structures of the inhibitors were imported into CERIUS2 as standard 3D single conformer representations in SD format. Subsequently, different descriptor groups were calculated for each compound employing the C2.DESCRIPTOR module of CERIUS2. The calculated descriptors included various simple and valence connectivity indices, electrotopological state indices, and other molecular descriptors (e.g., logarithm of partition coefficient, polarizability, dipole moment, molecular volume, molecular weight, molecular surface area, etc.).[34] The training compounds were fitted (using the best-fit option in CATALYST)[17] against the representative pharmacophores (14 models, Table 4), and their fit values were added as additional descriptors. The fit value for any compound is obtained automatically via eq 5.[17]

Genetic function approximation (GFA) was employed to search for the best possible QSAR regression equation capable of correlating the variations in biological activities of the training compounds with variations in the generated descriptors, i.e., multiple linear regression modeling (MLR). GFA techniques rely on the evolutionary operations of "crossover and mutation" to select optimal combinations of descriptors (i.e., chromosomes) capable of explaining bioactivity variation among training compounds from a large pool of possible descriptor combinations, i.e., chromosomes population. However, to avoid overwhelming GFA-MLR with a large number of poor descriptor populations, we removed lowest-variance descriptors (20%) prior to QSAR analysis.

Each chromosome is associated with a fitness value that reflects how good it is compared to other solutions. The fitness function employed herein is based on Friedman's "lack-of-fit" (LOF).[34]

Our preliminary diagnostic trials suggested the following optimal GFA parameters: explore linear, quadratic, and spline equations at mating and mutation probabilities of 50%, population size = 500, number of genetic iterations = 30000, and lack-of-fit (LOF) smoothness parameter = 1.0. However, to determine the optimal number of explanatory terms (QSAR descriptors), it was decided to scan and evaluate all possible QSAR models resulting from 10 to 24 explanatory terms.

All QSAR models were validated employing leave one-out cross-validation (r^2_{LOO}), bootstrapping (r^2_{BS}), and predictive r^2 (r^2_{PRESS}) calculated from the test subsets. The predictive r^2_{PRESS} is defined as:

$$r^2_{PRESS} = \text{SD-PRESS}/\text{SD} \quad (6)$$

where SD is the sum of the squared deviations between the biological activities of the test set and the mean activity of the training set molecules, and PRESS is the squared deviations between predicted and actual activity values for every molecule in the test set.

Descriptor-scanning identified several high-quality QSAR models, of which model C (Table 5) was selected as the best model to predict the inhibitory actions of our in silico hits. Two pharmacophore hypotheses emerged in this model, namely Hypo8/7 and Hypo4/9. Table 6 shows the three-dimensional coordinates of the two pharmacophores, while Figures 3 and 4 show the pharmacophoric features of the two models and how they map training compound 115 ($IC_{50} = 1.09$ nM) and the most potent hit compound 123 ($IC_{50} = 0.214$ μM). Figure 2 shows the plots of experimental versus fitted (training set) and predicted (testing set) HSL inhibitory bioactivities calculated from the QSAR model C (Table 5).

4.1.8. Addition of Exclusion Volumes. To account for the steric constrains of the binding pocket, we decided to decorate Hypo8/7 and Hypo4/9 with exclusion volumes employing HIPHOP-REFINE module of CATALYST. HIPHOP-REFINE uses inactive training compounds to construct excluded volumes that resemble the steric constrains of the binding pocket. It identifies spaces occupied by the conformations of inactive compounds and free from active ones. These regions are then filled with excluded volumes.[31]

Because each pharmacophore resembles a separate binding mode, it was decided to select two separate training subsets for constructing appropriate exclusion spheres around Hypo8/7 and Hypo4/9, namely subsets E and F, respectively (Tables 7 and 8, respectively).

In HIPHOP-REFINE, the user defines how many molecules must map completely or partially to the hypothesis via the principal and maximum omitted features (MaxOmitFeat) parameters. Active compounds are normally assigned MaxOmitFeat parameter of zero and principal value of 2 to instruct the software to consider all their chemical moieties in pharmacophore modeling and to fit them against all the pharmacophoric features of a particular hypothesis. On the other hand, inactive compounds are allowed to miss one (or two) features by assigning them a MaxOmitFeat of 1 (or 2) and principal value of zero.

We decided to consider 3.5 nM as an appropriate activity/inactivity threshold. Accordingly, inhibitors of IC_{50} values ≤ 3.5 nM were regarded as "actives" and were assigned principal and MaxOmitFeat values of 2 and 0, respectively, with few exceptions. On the other hand, inhibitors of $IC_{50} > 3.5$ nM were considered inactive and were assigned principal values of zero.[31] However, each inactive compound was carefully evaluated to assess whether its low potency is attributable to missing one or more pharmacophoric features, i.e., compared to active compounds, or related to possible steric clashes within the binding pocket, or due to both factors, i.e., the MaxOmitFeat parameter was set to 1 or 2. HIPHOP-REFINE was configured to allow a maximum of 100 exclusion spheres to be added to the generated pharmacophoric hypotheses. Tables 7 and 8 show the training compounds employed in this step and their corresponding principal and MaxOmitFeat parameters.

4.1.9. In Silico Screening for New HSL Inhibitors. The sterically refined versions of Hypo4/9 and Hypo8/7 were employed as 3D search queries to screen two 3D flexible structural databases, namely NCI list of compounds and our *in-house* built database of known drugs and agrochemicals. Screening was performed employing the "Best Flexible Database Search" option implemented within CATALYST. Hits retrieved from the NCI database were filtered using Lipinski's and Veber's rules.

Hits from both searches were fitted against the two pharmacophores using the "best fit" option within CATALYST. The fit values together with the relevant molecular descriptors of each hit were substituted in the optimal QSAR eq 1. The highest ranking molecules based on QSAR predictions were acquired and tested in vitro. Table 9 shows their QSAR-predictions and experimental bioactivities.

4.2. In Vitro Experimental Studies. 4.2.1. Materials. Wistar male rats, weighing between 140−200 g and fed ad libitum with standard feed and water were cared for in the animal laboratory at faculty of Pharmacy at the University of Jordan. Materials were purchased from corresponding companies (in brackets) and were used in the experimentation without further purification: Krebs Ringer bicarbonate (KRB, Sigma, USA), bovine serum albumin (BSA, Sigma, USA), dimethyl sulfoxide (DMSO, BDH Laboratory Supplies, England), Tris base (Promega Corporation, USA), collagenase (Sigma, USA), protease inhibitors tablet (SIGMA*FAST*, Sigma, USA), *p*-nitrophenyl butyrate (PNPB, Sigma, USA), dithioerythritol (DTT, Fluka, Switzerland), bifenox (Riedel-de Haen, Germany), chlorfenson (Riedel-de Haen, Germany), esfenvalerate (Riedel-de Haen, Germany), fenvalerate (Riedel-de Haen, Germany), fenpropathrin (Riedel-de Haen, Germany), ethiofencarb (Riedel-de Haen, Germany), silafluofen (Riedel-de Haen, Germany), oxybenzone (Riedel-de Haen, Germany), capsaicin (Sigma, USA), naproxen (Fluka, USA), dibenzoylmethane (Fluka, Germany), benzyl benzoate (Medex, England). NCI hits were kindly donated from the National Cancer Institute.

4.2.2. Extraction of the HSL Enzyme. Isolated fat cells were extracted from rat epididymal adipose tissues as described earlier.[42] Briefly, Wistar male rats were sacrificed by cervical dislocation, and their epididymal fat pads were removed quickly and rinsed several times in normal saline. The tissue was weighed and minced into small pieces and placed in a flask. The resulting mass was treated as follows: for each 1.0 g of tissue, 3 mL of KRB (pH 7.4) supplemented with 4% BSA were added, followed by 10 mg of collagenase. The mixture was incubated and agitated in a metabolic shaker (Shaking Incubator, Daiki Scientific Corporation) over 2 h at 37 °C. Subsequently, fat cells were liberated from the tissue fragments by gentle stirring with a rod.

The resulting suspension was centrifuged for 1 min at 400*g* at 20 °C. Fat cells floated to the surface while stromal-vascular cells settled at the bottom. Stromal-vascular cells were removed by aspiration. Fat cells were decanted and washed by suspending them in 10 mL of warm (37 °C) KRB-BSA solution followed by centrifugation (for 1 min at 400*g* at 20 °C) and a second round of removing stromal-vascular cells by aspiration. This washing procedure was repeated three times.

HSL was extracted from epididymal fat cells as reported earlier.[43] Briefly, 1 mL of suspended fat cells (in KRB-BSA solution) was further diluted by 2.5 mL KRB-BSA and incubated at 37 °C for 30 min. Subsequently, the suspension was centrifuged at 100*g* for 1 min to separate the infranatant from the fat cells.

For each 1.0 mL of suspended fat cells, a 1.125 mL homogenization buffer (each 100 mL prepared from 50 mM Tris-HCl, pH 7.0, 250 mM sucrose, and 1 crushed protease inhibitor tablet) was added and the mixture was manually agitated 20 times. The homogenate was centrifuged at 4540*g* and 4 °C over 10 min. Subsequently, 250 μL of diethyl ether was added to the homogenate and abruptly shaken and centrifuged at 1200*g* over 5 min at 4 °C. The upper ether layer was aspirated. The subsequent supernatant was used as HSL extract. HSL extract aliquots (0.5 mL) were stored in Epindruff tubes at −80 °C for later use.

4.2.3. Preparation of Hit Compounds for In Vitro Assay. The tested compounds were provided as dry powders in variable quantities (5 mg to 100 g). They were initially dissolved in DMSO to give stock solutions of 20 or 50 mM. Subsequently, they were diluted to the required concentrations with phosphate buffer (pH 7.25; 0.1 M NaH_2PO_4; 0.9% NaCl and 1.0 mM dithioerythritol) for enzymatic assay.

4.2.4. Quantification of HSL Activity in a Spectrophotometric Assay. The lipase activity of HSL was quantified by a colorimetric assay that measures the release of *p*-nitrophenol as previously described.[12] However, *p*-nitrophenyl butyrate (PNPB) was employed as HSL substrate at 10 μM in the enzymatic assays instead of 5 mM.[12] HSL extract (0.10 mL) was added to the reaction mixtures. The volume was completed to 1 mL using phosphate buffer before measuring the solution absorbances spectrophoto-

metrically at λ of 400 nm at three time points: 1, 3, and 6 min. The reactions were maintained at 37 °C.

4.2.5. HSL Inhibition by Hit Compounds. The inhibition of HSL lipase activity by hit compounds was measured using the spectrophotometric assay described above. HSL was preincubated with 10 μM or 1 μM of each particular hit compound for 30 min at 37 °C before adding the substrate. The final concentration of DMSO did not exceed 1.0%. The percentage of residual activity of HSL was determined for each compound by comparing the lipase activity of HSL with and without the compound. The concentration required to give 50% inhibition (IC_{50}) was determined for the nine compounds having the best inhibitory activities. HSL was preincubated with different concentrations of the selected compounds (**123**, **127**, **129**, **132**, **148**, **153**, **155**, **157**, and **159**, Table 9) and the percentages of residual activity of HSL data were used to evaluate the IC_{50} values.

Acknowledgment. This project was partially sponsored by the Faculty of Graduate Studies (M.Sc. Thesis of Lina Ali Dahabiyeh). We thank the Deanship of Scientific Research and Hamdi-Mango Center for Scientific Research at the University of Jordan for their generous funds. We also thank the National Cancer Institute for kindly donating compounds for testing.

Supporting Information Available: Descriptor values of eq 1, purity information. This material is available free of charge via the Internet at http://pubs.acs.org.

References

(1) Bailey, C. J. Potential new treatments for type 2 diabetes. *TiPS* **2000**, *21*, 259–265.
(2) Miles, J. M.; Nelson, R. H. Contribution of triglyceride-rich lipoproteins to plasma free fatty acids. *Horm. Metab. Res.* **2007**, *39*, 726–729.
(3) Frayn, K. N. Adipose tissue as a buffer for daily lipid flux. *Diabetologia* **2002**, *45*, 1201–1210.
(4) Kim, J. K.; Fillmore, J. J.; Chen, Y.; Yu, C.; Moore, I. K.; Pypaert, M.; Lutz, E. P.; Kako, Y.; Velez-Carrasco, W.; Goldberg, I. J.; Breslow, J.; Schulman, G. I. Tissue-specific over expression of lipoprotein lipase causes tissue-specific insulin resistance. *Proc. Natl. Acad. Sci. U.S.A.* **2001**, *98*, 7522–7527.
(5) Pfeiffer, A. F. Adipose tissue and diabetes therapy: do we hit the target? *Horm. Metab. Res.* **2007**, *39*, 734–738.
(6) Kraemer, F. B.; Shen, W. Hormone-Sensitive Lipase Knockouts. *Nutr. Metab.* **2006**, *12*, 1–7.
(7) Lowe, D. B.; Magnuson, S.; Oi, N.; Campbell, A.; Cook, J.; Hong, Z.; Wang, M.; Rodriguez, M.; Achebe, F.; Kluender, H.; Wong, W. C.; Bullock, W. H.; Salhanick, A.I. ; Witman, J. T.; Bowling, M. E.; Keiperb, C.; Clairmont, K. B. In vitro SAR of (5-(2*H*)-isoxazolonyl) ureas, potent inhibitors of hormone-sensitive lipase. *Bioorg. Med. Chem. Lett.* **2004**, *14*, 3155–3159.
(8) Jianping, Y. Role of Insulin in the Pathogenesis of Free Fatty Acid-Induced Insulin Resistance in Skeletal Muscle. *Endocr. Metab. Immune Disord.: Drug Targets* **2007**, *7*, 65–74.
(9) Holm, C. Molecular mechanisms regulating hormone-sensitive lipase and lipolysis. *Biochem. Soc. Trans.* **2003**, *31*, 1120–1124.
(10) Ebdrup, S.; Sorensen, L. G.; Olsen, O. H.; Jacobsen, P. Synthesis and Structure−Activity Relationship for a Novel Class of Potent and Selective Carbamoyl-Triazole Based Inhibitors of Hormone Sensitive Lipase. *J. Med. Chem.* **2004**, *47*, 400–410.
(11) Ebdrup, S.; Hoffmann, H.; Refsgaard, F.; Fledelius, C.; Jacobsen, P. Synthesis and Structure−Activity Relationship for a Novel Class of Potent and Selective Carbamate-Based Inhibitors of Hormone Selective Lipase with Acute in Vivo Antilipolytic Effects. *J. Med. Chem.* **2007**, *50*, 5449–5456.
(12) Slee, D. H.; Bhat, A. S.; Nguyen, T. N.; Kish, M.; Lundeen, K.; Newman, M. J.; McConnell, S. J. Pyrrolopyrazinedione-Based Inhibitors of Human Hormone-Sensitive Lipase. *J. Med. Chem.* **2003**, *46*, 1120–1122.
(13) Shoenafinger, K.; Petry, S.; Mueller, G.; Barringhous, K.-H. PCT Appl. WO 0166533, 2001.
(14) Petry, S.; Schoenafinger, K.; Mueller, G.; Barringhous, K.-H. PCT Appl. WO 0117981, 2001.
(15) De Jong, J. C.; Sorensen, L. G.; Tornqvistc, H.; Jacobsen, P. Carbazates as potent inhibitors of hormone-sensitive lipase. *Bioorg. Med. Chem. Lett.* **2004**, *14*, 1741–1744.
(16) Ebdrup, S.; Jacobsen, P.; Dhanda Farrington, A.; Vedsø, P. Structure−activity relationship for aryl and heteroaryl boronic acid inhibitors of hormone-sensitive lipase. *Bioorg. Med. Chem.* **2005**, *13*, 2305–2312.
(17) *CATALYST 4.11 Users' Manual*; Accelrys Software Inc.: San Diego, CA, 2005.
(18) Sprague, P. W.; Hoffmann, R. In *Computer Assisted Lead Finding and Optimization. Current Tools for Medicinal Chemistry*; Van de Waterbeemd, H., Testa, B., Folkers, G., Eds.; VHCA: Basel, Switzerland, 1997; pp 230−240.
(19) Barnum, D.; Greene, J.; Smellie, A.; Sprague, P. Identification of common functional configurations among molecules. *J. Chem. Inf. Comput. Sci.* **1996**, *36*, 563–571.
(20) Smellie, A.; Teig, S.; Towbin, P. Polling: Promoting Conformational Variation. *J. Comput. Chem.* **1995**, *16*, 171–187.
(21) Li, H.; Sutter, J.; Hoffmann, R. In *Pharmacophore Perception, Development, and Use in Drug Design*; Güner, O. F., Ed.; International University Line: La Jolla, CA, 2000; pp 173−189.
(22) Sutter, J.; Güner, O.; Hoffmann, R.; Li, H.; Waldman, M. In *Pharmacophore Perception, Development, and Use in Drug Design*; Güner, O. F., Ed.; International University Line: La Jolla, CA, 2000; pp 501−511.
(23) Kurogi, Y.; Guner, O. F. Pharmacophore modeling and three dimensional database searching for drug design using catalyst. *Curr. Med. Chem.* **2001**, *8*, 1035–1055.
(24) Bersuker, I. B.; Bahçeci, S.; Boggs, J. E. In *Pharmacophore Perception, Development, and Use in Drug Design*; Güner O. F., Ed.; International University Line: La Jolla, CA, 2000; pp 457−473.
(25) Poptodorov, K.; Luu, T.; Langer, T.; Hoffmann, R. In *Methods and Principles in Medicinal Chemistry. Pharmacophores and Pharmacophores Searches*; Hoffmann, R. D., Ed.; Wiley-VCH: Weinheim, Germany, 2006; Vol. 2, pp 17−47.
(26) Singh, J.; Chuaqui, C. E.; Boriack-Sjodin, P. A.; Lee, W. C.; Pontz, T.; Corbley, M. J.; Cheung, H. K.; Arduini, R. M.; Mead, J. N.; Newman, M. N.; Papadatos, J. L.; Bowes, S.; Josiah, S.; Ling, L. E. Successful shape-based virtual screening: the discovery of a potent inhibitor of the type I TGFbeta receptor kinase (TbetaRI). *Bioorg. Med. Chem. Lett.* **2003**, *13*, 4355–4359.
(27) Taha, M. O.; Qandil, A. M.; Zaki, D. D.; AlDamen, M. A. Ligand-based assessment of factor Xa binding site flexibility via elaborate pharmacophore exploration and genetic algorithm-based QSAR modeling. *Eur. J. Med. Chem.* **2005**, *40*, 701–727.
(28) Taha, M. O.; Bustanji, Y.; Al-Ghussein, M. A. S.; Mohammad, M.; Zalloum, H.; Al-Masri, I. M.; Atallah, N. Pharmacophore Modeling, Quantitative Structure−Activity Relationship Analysis and In Silico Screening Reveal Potent Glycogen Synthase Kinase-3β Inhibitory Activities for Cimetidine, Hydroxychloroquine and Gemifloxacin. *J. Med. Chem.* **2008**, *51*, 2062–2077.
(29) Taha, M. O.; Atallah, N.; Al-Bakri, A. G.; Paradis-Bleau, C.; Zalloum, H.; Younis, K.; Levesque, R. C. Discovery of New MurF Inhibitors via Pharmacophore Modeling and QSAR Analysis followed by in silico screening. *Bioorg. Med. Chem.* **2008**, *16*, 1218–1235.
(30) Taha, M. O.; Al-Bakri, A. G.; Zalloum, W. A. Discovery of potent inhibitors of pseudomonal quorum sensing via pharmacophore modeling and in silico screening. *Bioorg. Med. Chem. Lett.* **2006**, *16*, 5902–5906.
(31) Taha, M. O.; Bustanji, Y.; Al-Bakri, A. G.; Yousef, M.; Zalloum, W. A.; Al-Masri, I. M.; Atallah, N. Discovery of new potent human protein tyrosine phosphatase inhibitors via pharmacophore and QSAR analysisfollowed by in silico screening. *J. Mol. Graphics Modell.* **2007**, *25*, 870–884.
(32) Sheridan, R. P.; Kearsley, S. K. Why do we need so many chemical similarity search methods? *Drug Discovery Today* **2002**, *7*, 903–911.
(33) Fischer, R. *The Principle of Experimentation Illustrated by a Psycho-Physical Experiment*, 8th ed.; Hafner Publishing: New York, 1966; Chapter II.
(34) *CERIUS2, QSAR Users' Manual*, version 4.10; Accelrys Inc.: San Diego, CA, 2005; pp 43−88, 221−235.
(35) Ramsey, L. F.; Schafer, W. D. *The Statistical Sleuth*, 1st ed.; Wadsworth Publishing Company: Belmont, CA, 1997.
(36) Clement, O. O.; Mehl, A. T. Pharmacophore Perception, Development, and Use in Drug Design. In *IUL Biotechnology Series*; Guner, O. F., Ed.; International University Line: La Jolla, CA, 2000; pp 71−84.
(37) Lipinski, C. A.; Lombardo, F.; Dominy, B. W.; Feeney, P. J. Experimental and computational approaches to estimate solubility and permeability in drug discovery and development settings. *Adv. Drug Delivery Rev.* **2001**, *46*, 3–26.
(38) Veber, D. F.; Johnson, S. R.; Cheng, H. Y.; Smith, B. R.; Ward, K. W.; Kopple, K. D. Molecular properties that influence the oral bioavailability of drug candidates. *J. Med. Chem.* **2002**, *45*, 2615–2623.
(39) European Food Safety Authority. Conclusion regarding the peer review of the pesticide risk assessment of the active substance, bifenox. *Sci. Rep.* **2007**, *119*, 1−84.

(40) Langin, D.; Laurell, H.; Holst, L. S.; Belfrage, P.; Holm, C. Gene organization and primary structure of human hormonesensitive lipase: possible significance of a sequence homology with a lipase of Moraxella TA144, an antarctic bacterium. *Biochem. J.* **1993**, *90*, 4897–4901.

(41) Krovat, E. M.; Langer, T. Non-Peptide Angiotensin II Receptor Antagonists: Chemical Feature Based Pharmacophore Identification. *J. Med. Chem.* **2003**, *46*, 716–726.

(42) Rodbell, M. Metabolism of Isolated Fat Cells. *J. Biol. Chem.* **1964**, *293*, 375–380.

(43) Morimoto, C.; Sumiyoshi, M.; Kameda, K.; Tsujita, T.; Okuda, H. Relationship between Hormone-Sensitive Lipolysis and Lipase Activity in Rat Fat Cells. *J. Biochem.* **1999**, *125*, 976–981.

(44) Petry, S.; Baringhaus, K. H.; Schoenafinger, K.; Jung, C.; Kleine, H.; Müller, G. HTS of Hormone sensitive Lipase and Subsequent Computer-assisted Compound Optimization. In *Lipases and Phospholipases in Drug Development*; Mueller, G., Petry, S., Eds.; Wiley-VCH Verlag GmbH & Co. KGaA: Weinheim, 2004; pp 121−137.

JM800718K